Journal of Materials Chemistry A

RSC Publishing

PAPER

View Article Online
View Journal | View Issue

Ternary sulfur/polyacrylonitrile/$Mg_{0.6}Ni_{0.4}O$ composite cathodes for high performance lithium/sulfur batteries

Cite this: *J. Mater. Chem. A*, 2013, **1**, 295

Yongguang Zhang,[a] Yan Zhao,[a] Assiya Yermukhambetova,[b] Zhumabay Bakenov[b] and P. Chen*[a]

Nanostructured magnesium nickel oxide ($Mg_{0.6}Ni_{0.4}O$) was synthesized by a self-propagating high temperature synthesis method followed by heat treatment. The particles of the resulting oxide were used as additives to prepare the sulfur/polyacrylonitrile/$Mg_{0.6}Ni_{0.4}O$ (S/PAN/$Mg_{0.6}Ni_{0.4}O$) composite *via* wet ballmilling. The SEM observation revealed that the composite morphology was drastically changed by the addition of $Mg_{0.6}Ni_{0.4}O$, from smooth bulky particles of S/PAN to rough nanostructured agglomerates with two times the increase in the specific surface area, favouring the reactivity of the composite, and a homogeneous component distribution. Cyclic voltammetry, discharge–charge tests and ac impedance spectroscopy have shown improved conductivity and electrochemical properties of the composite by the addition of $Mg_{0.6}Ni_{0.4}O$, leading to high sulfur utilization and interfacial stabilization in a Li/S cell upon discharge–charge cycling. The cell demonstrated enhanced reversibility, resulting in a discharge capacity of about 1223 mA h g^{-1} at the second cycle and retained about 100% of this value over 100 cycles. Furthermore, the S/PAN/$Mg_{0.6}Ni_{0.4}O$ composite cathode exhibited a good rate capability with discharge capacities of 887, 710 and 445 mA h g^{-1} at 0.5, 0.7 and 1 C, respectively.

Received 29th August 2012
Accepted 5th October 2012

DOI: 10.1039/c2ta00105e

www.rsc.org/MaterialsA

Introduction

Lithium-ion batteries are leading the path of power sources for portable applications from small consumer electronics to electricity powered transport. Despite this, their wider application is restricted due to the limited energy density of available cathode materials. The lithium/sulfur (Li/S) system, based on the electrochemical reaction $16Li + S_8 \leftrightarrow 8Li_2S$, is one of the most promising candidates for high energy density applications, especially in electric vehicles (EVs) and hybrid electric vehicles (HEVs), due to its low cost, environment friendliness, large theoretical specific capacity and energy of 1672 mA h g^{-1} and 2500 W h kg^{-1}, respectively.[1–3] However, the development of the lithium/sulfur battery has been hindered to date by a series of challenges.[4–9] The insulating nature of S, large volume change during intercalation processes and solubility of polysulfides as intermediate products in liquid electrolytes are the most serious barriers in its way to practical application as a cathode material in lithium rechargeable batteries.

Various methods to address the above issues have been explored, including addition of various types of conductive carbon materials[6,10–21] and conductive polymers,[22–26] in order to enhance the electronic conductivity of the composite and hinder the dissolution of polysulfides into the electrolyte.

Among different types of composites, the sulfur/polyacrylonitrile (S/PAN) composite has demonstrated high sulfur utilization and large capacity at initial cycles.[23] However, the poor electronic conductivity of the S/PAN binary composite hinders the cyclability and the performance at high C-rates. It is noted that Li/S batteries exhibit enhanced electrochemical performance with different kinds of additives to the sulfur cathode, which results in a change in morphology and/or absorbing properties.[27–29] These additives have advantages of small dosage and fast effect without increasing the cost of battery compared with the other technologies.[30] Therefore, employment of additives in the Li/S batteries to enhance the performance by modifying the morphology of the S composite is an effective approach in preparing high performance sulfur cathodes.

In this work, we report on the preparation of nanosized $Mg_{0.6}Ni_{0.4}O$ *via* a self-propagating high temperature synthesis (SHS) method, its effect on the electrochemical performance of the S/PAN/$Mg_{0.6}Ni_{0.4}O$ ternary composite cathode, and characterization of the composites physical and electrochemical properties as a cathode for lithium secondary batteries.

Experimental

The synthesis of $Mg_{0.6}Ni_{0.4}O$ was carried out by the SHS method. 0.6 mol $Mg(NO_3)_2$ (Sigma-Aldrich, 98% purity), 0.4 mol

[a]*Department of Chemical Engineering, University of Waterloo, 200 University Avenue West, Waterloo, Ontario, N2L 3G1 Canada. E-mail: p4chen@uwaterloo.ca; Fax: +1 519 746 4979; Tel: +1 519 888 4567 extn 35586*

[b]*School of Engineering, Nazarbayev University, 53 Kabanbay Batyr Avenue, Astana 010000, Kazakhstan. E-mail: zbakenov@nu.edu.kz*

$Ni(NO_3)_2$ (Sigma-Aldrich, 98% purity) and 3.5 mol glycine (Fisher Scientific, 98.5% purity) were dissolved in 0.100 dm^3 deionized water. The solution was boiled on a hot plate with stirring to evaporate excess water. The resulting viscous liquid ignited and underwent self-sustaining combustion, producing an ash composed of nickel and magnesium oxide products. The solid samples were calcined at 700 °C for 6 h in air and the resulting $Mg_{0.6}Ni_{0.4}O$ powders were ground in an agate mortar.

The ternary composite preparation is schematically presented in Fig. 1. Sulfur (Sigma-Aldrich, 100-mesh particle size powder), polyacrylonitrile (PAN) (Sigma-Aldrich) and as-prepared $Mg_{0.6}Ni_{0.4}O$ were mixed in the weight ratio of 4 : 1 : 0.25 and ball milled (Fritsch, Pulverisette 7 Classic Line) at 800 rpm for 2 h with ethanol as a dispersant. The precursor mixture was further dried in a vacuum oven at 60 °C for 3 h to remove the solvent and then heat treated at 350 °C for 3 h in a tubular furnace in Ar gas to melt sulfur and react it with PAN.[10] For comparison with the ternary composite, the S/PAN binary composite cathode was prepared in the same way.

The crystalline phases of the samples were determined using an X-ray diffractometer (XRD, D8 Discover, Bruker) equipped with Cu-Kα radiation and a high resolution transmission electron microscope (HRTEM, FEI TITAN 80-300) equipped with selected area electron diffraction (SAED). The sample surface morphology was examined by field emission scanning electron microscopy (FE-SEM, Leo-1530, Zeiss). The specific surface area was determined by the Brunauer–Emmett–Teller method (BET, ASAP 2020, Micromeritics). The S content of the samples was determined by chemical analysis (CHNS, Vario Micro Cube, Elementar). The interior structure of samples was observed using a transmission electron microscope (TEM, CM10, Philips) at 60 kV and a high resolution transmission electron microscope (HRTEM, FEI TITAN 80-300) equipped with Energy Dispersive Spectroscopy (EDS).

CR2032 coin-type cells were assembled inside a MBRAUN glove box filled with high purity argon (99.9995% purity) by sandwiching a polypropylene separator (Celgard, USA) between the composite cathode and lithium anode, and using 1 mol dm^{-3} lithium hexafluorophosphate ($LiPF_6$) in ethylene carbonate (EC) : dimethyl carbonate (DMC) : diethyl carbonate (DEC) = 1 : 1 : 1 as an electrolyte (EMD chemicals Inc., Selectlyte battery electrolyte LP40). The cathode was comprised of 80 wt% binary or ternary composite, 10 wt% acetylene black (AB, MTI Co) as a conductive material and the rest was polyvinylidene fluoride (PVdF, Kynar, HSV900) as a binder. These materials were dispersed in *n*-methyl-2-pyrrolidinone (NMP, Sigma-Aldrich). The resultant slurry was spread onto a circular nickel foam (MTI, ≥99% purity) of 1 cm diameter and then dried in vacuum for 12 h at 60 °C. Finally, the electrode was pressed at 8 MPa using a hydraulic press in order to achieve good contact between the active material and the nickel foam current collector. The electrodes were prepared to make their weight and thickness the same by precise weighing, pressing and controlling their geometry. The cathode material loading in each electrode was about 4 mg cm^{-2}, and the thickness of the electrode film was about 100 μm. The cells were tested galvanostatically on multi-channel battery testers (BT-2000, Arbin) between 1 and 3 V *vs.* Li^+/Li at different current densities, and specific capacities were calculated on the basis of the weight of S in the composite cathode.

Cyclic voltammetry (CV) was performed by means of a potentiostat/galvanostat (VMP3, Biologic) between 1 and 3 V *vs.* Li^+/Li at a scanning rate of 0.1 mV s^{-1}. The electrochemical impedance spectroscopy (EIS) measurements were carried out using a potentiostat/galvanostat VMP3 by applying an ac voltage of 10 mV over the frequency range of 0.1 Hz to 1 MHz. All electrochemical measurements were performed at room temperature.

Results and discussion

The XRD analysis was used to investigate potential structural changes due to the starting material interactions including possible reactions of $Mg_{0.6}Ni_{0.4}O$ with other cathode components. Fig. 2 shows the XRD patterns of the starting components S, the as-prepared $Mg_{0.6}Ni_{0.4}O$ and the S/PAN/$Mg_{0.6}Ni_{0.4}O$ ternary composite. One can see that the XRD patterns of the S/PAN/$Mg_{0.6}Ni_{0.4}O$ ternary composite have sharp peaks of a face-centered cubic structure $Mg_{0.6}Ni_{0.4}O$ with a reduced peak intensity compared with those of the initial $Mg_{0.6}Ni_{0.4}O$. On the other hand, the characteristic *Fddd* orthorhombic crystal structure peaks of elemental sulfur disappear from the XRD

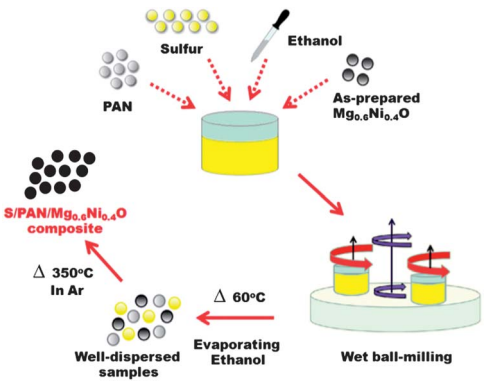

Fig. 1 Schematic of preparation of the S/PAN/$Mg_{0.6}Ni_{0.4}O$ ternary composite.

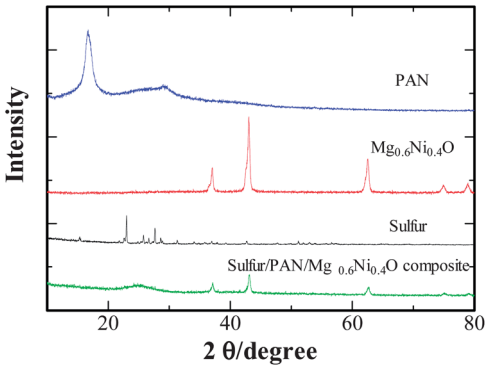

Fig. 2 XRD patterns of the starting components S, PAN, as-prepared $Mg_{0.6}Ni_{0.4}O$ and S/PAN/$Mg_{0.6}Ni_{0.4}O$ ternary composite.

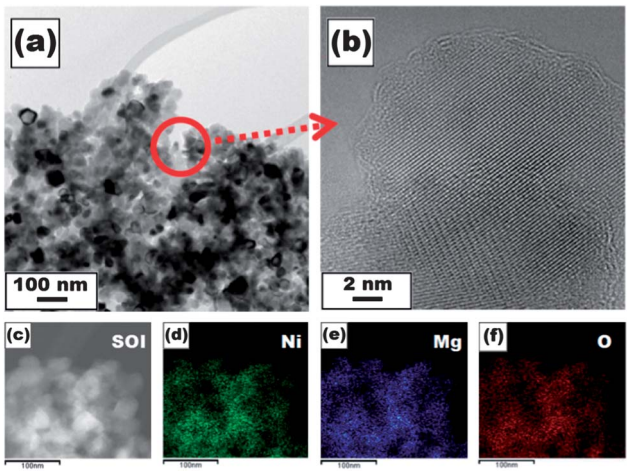

Fig. 3 HRTEM images of $Mg_{0.6}Ni_{0.4}O$ samples at different magnifications (a and b); EDS mapping showing the distribution of Mg, Ni and O elements (c–f).

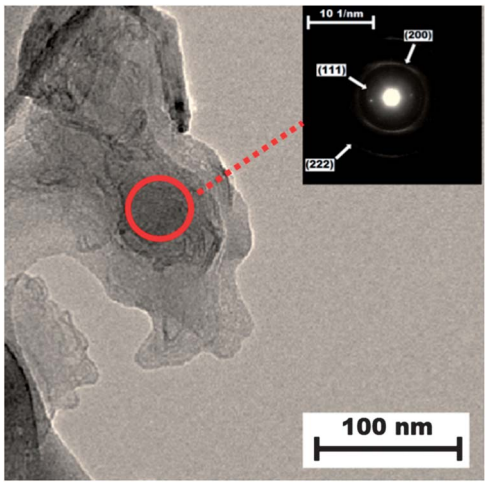

Fig. 5 HRTEM image and SAED pattern of the S/PAN/$Mg_{0.6}Ni_{0.4}O$ ternary composite.

patterns of the ternary composite, which could be due to the trapping of S into the internal structure of the composite. The XRD data do not show any new phases in the final product, which could be an indication of the absence of chemical reaction between the composite components upon ball-milling and the following heat treatment. Chemical analysis has shown that the sulfur content in the S/PAN/$Mg_{0.6}Ni_{0.4}O$ ternary composite was 38.5 wt%.

Fig. 3a presents the HRTEM images of the $Mg_{0.6}Ni_{0.4}O$ particles. The sample is nanostructured and consists of primary particles ranging from 20–50 nm. At a higher magnification (Fig. 3b), obvious lattice fringes could be observed, and $Mg_{0.6}Ni_{0.4}O$ had a highly crystalline structure, which is consistent with the XRD results. The EDS mapping (Fig. 3c–f) confirmed the homogeneous dispersion of Ni, Mg and O elements in the $Mg_{0.6}Ni_{0.4}O$ bulk.

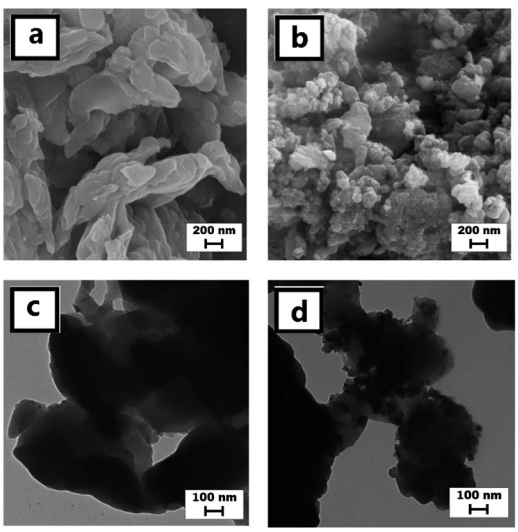

Fig. 4 SEM images and TEM images of (a and c) S/PAN binary and (b and d) S/PAN/$Mg_{0.6}Ni_{0.4}O$ ternary composites.

The effect of the $Mg_{0.6}Ni_{0.4}O$ nanoparticle in addition to the composite morphology could be observed from the SEM data presented in Fig. 4(a) and (b). It is noted that the surface morphology of the S/PAN binary composite changes significantly by addition of about 4 wt% of $Mg_{0.6}Ni_{0.4}O$ nanoparticles. Fig. 4a shows typical S/PAN nanostructures containing agglomerated particles with diameters ranging from 0.1 μm to 1 μm. It can be seen that the S/PAN composite is bulk and its particles are very compact and has smooth surface, while the S/PAN/$Mg_{0.6}Ni_{0.4}O$ ternary composite consists of nanosized primary particles resulting in a rough surface of the ternary composite. The BET specific surface area of this composite was 17.1 $m^2\ g^{-1}$, which is two times higher than that of the S/PAN composite of 8.0 $m^2\ g^{-1}$, which could be beneficial for the contact and interaction between the electrode and the electrolyte. On the other hand, the ternary composite contains many nanosized particles, creating a 3D porous nanostructure, which could be highly favourable for the ion diffusivity and improve the cathode electrochemical performance in Li/S batteries.

The comparison of the TEM results of the binary and ternary composites (Fig. 4c and d) shows the well-dispersed dark spots in the ternary composite. The "dark dots" are the $Mg_{0.6}Ni_{0.4}O$ particles embedded in the composite bulk, which was confirmed by HRTEM equipped with SAED (Fig. 5). The SAED pattern in this phase, shown in Fig. 5, consists of a few rings which could be assigned to the face-centered cubic structure of

Table 1 *d*-Spacing derived from SAED analysis of the as-prepared $Mg_{0.4}Ni_{0.6}O$

As-prepared	$Mg_{0.4}Ni_{0.6}O$[a]	
nm	Nm	*d*(*hkl*)
0.236	0.242	(111)
0.202	0.209	(200)
0.119	0.121	(222)

[a] JCPDS 34-0410.

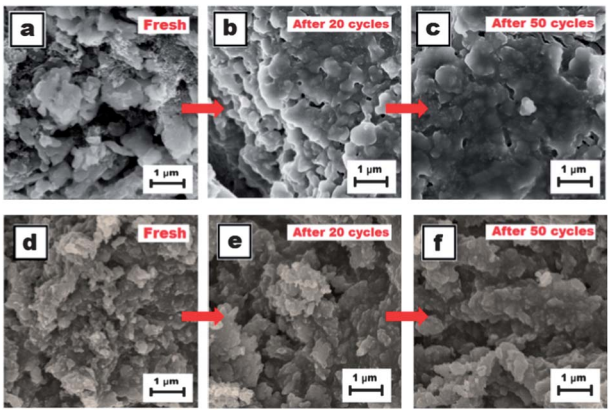

Fig. 6 SEM images of (a–c) binary and (d–f) ternary composites before and after discharge–charge cycles.

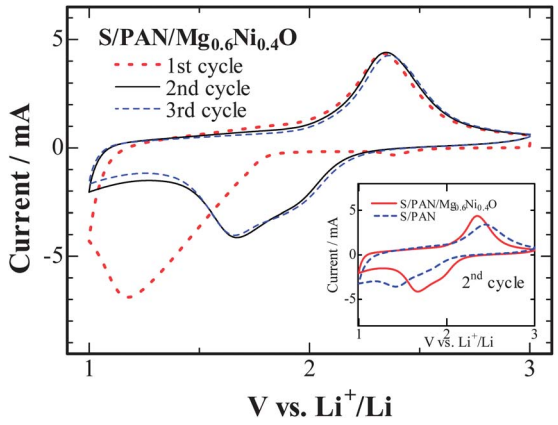

Fig. 8 CV profiles of lithium cells with the binary and ternary composite cathodes. Scan rate 0.1 mV s^{-1}.

$Mg_{0.6}Ni_{0.4}O$. All *d*-spacing derived from SAED spectra are shown in Table 1. This agrees well with the sharp peaks in the XRD patterns.

Fig. 6 shows the SEM images of fresh and cycled binary and ternary composite cathodes. It can be seen from Fig. 6a–c that the S/PAN binary cathode morphology drastically changes upon cycling, and the active material particles in the binary composite continuously merge into a large solid bulk, which could be due to the separation of active materials from the conducting agent and binder and further agglomeration into low conductive S/PAN particles, negatively affecting the cathode conductivity and sulfur utilization. This process becomes stronger upon further cycling resulting in severe agglomeration of the active cathode material, which could be one of the major reasons for poor cyclability of the S/PAN binary composite cathode. In contrast, the morphology of the S/PAN/$Mg_{0.6}Ni_{0.4}O$ ternary composite does not change remarkably even after 50 cycles (see Fig. 6d–f) and keeps its nanostructured feature.

The SEM results presented in Fig. 6 allow us to suggest that the $Mg_{0.6}Ni_{0.4}O$ suppresses the separation and agglomeration of active materials in the composite, which enhances the cathode stability and its electrochemical performance. The morphology changes of both the binary and ternary composite cathodes during discharge–charge are schematically represented in Fig. 7. In the binary sulfur composite, sulfur does not remain fixed in its original position and its distribution cannot remain homogeneous upon cycling as reported by Jeon *et al.*[31] By adding $Mg_{0.6}Ni_{0.4}O$, the as-prepared ternary composite is enabled to maintain homogeneous distribution of its components and unchanged morphology during discharge–charge cycling, and retain the reactive sites in its nanosized structure.

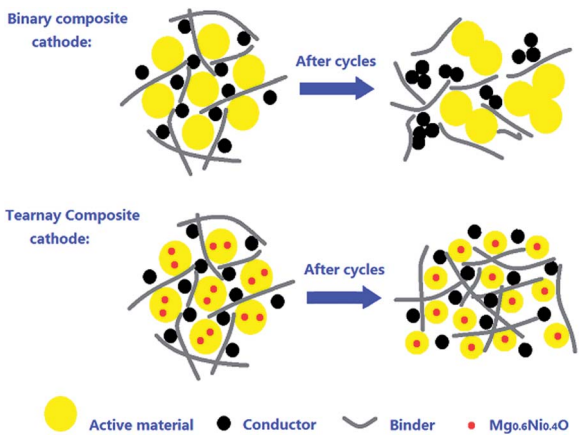

Fig. 7 Schematic model of the morphology change in the composite cathode during discharge–charge cycling.

Fig. 8 shows the initial CV cycles of the S/PAN/$Mg_{0.6}Ni_{0.4}O$ ternary composite. The CV data confirm that the $Mg_{0.6}Ni_{0.4}O$ additive is not electrochemically active in the selected voltage region. One can see that at the initial cycle there is a pronounced reduction process, which could be due to the side reactions of formation of the solid electrolyte interface (SEI), and these processes lead to a larger polarization between the reduction and oxidation peaks. It could be suggested that these processes are inherent only for the first cycle because they are not present in the following CV cycles as it can be seen from Fig. 8. The inset of Fig. 8 presents the comparison of the electrochemical responses of Li/S cells with the S/PAN and S/PAN/$Mg_{0.6}Ni_{0.4}O$ composites at the second CV cycle. It can be seen that both binary and ternary composites evidence two major stages of the redox processes in the system which agrees with the literature data,[26,32,33] and could be attributed to the transition of S to polysulfides (Li_2S_8, Li_2S_6, Li_2S_4, Li_2S_2), and their further transformation into lithium sulfide (Li_2S), respectively. Furthermore, it can be seen that the as-prepared $Mg_{0.6}Ni_{0.4}O$ as an additive leads to the enhanced electrochemical response of the cathode. The ternary composite S/PAN/$Mg_{0.6}Ni_{0.4}O$ had a pair of well distinguished redox peaks separated by about 0.67 V. The corresponding peaks of the binary S/PAN composite are weaker and broader, and the voltage gap between them is about 1.04 V. These observations allow us to suggest that the addition of $Mg_{0.6}Ni_{0.4}O$ leads to the enhanced electrochemical kinetics of the sulfur cathode resulting in the reduced polarization of the electrodic processes on the S/PAN/$Mg_{0.6}Ni_{0.4}O$ composite cathode. This performance enhancement could be attributed to the enhanced charge transfer of the material due

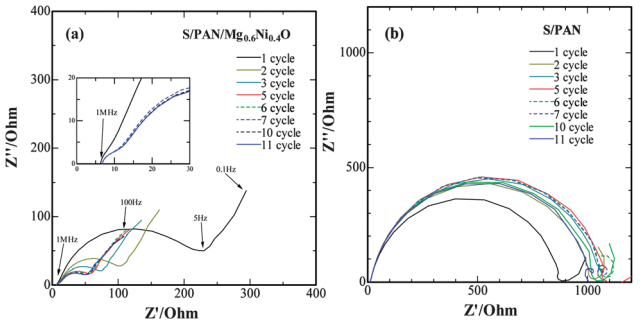

Fig. 9 EIS data for fresh and cycled lithium cells with (a) ternary S/PAN/$Mg_{0.6}Ni_{0.4}O$ (inset: enlarged image of the high frequency part of EIS for S/PAN/$Mg_{0.6}Ni_{0.4}O$) and (b) binary S/PAN composite cathodes.

to the addition of $Mg_{0.6}Ni_{0.4}O$. The observed morphology advantages and stability of the ternary composite could provide a larger electrode–electrolyte interface, reducing the charge transfer resistance at this boundary.

EIS is a powerful tool to study such interfacial effects. The EIS measurements of the lithium half-cells with S/PAN and S/PAN/$Mg_{0.6}Ni_{0.4}O$ composite cathodes were carried out before and after the galvanostatic discharge–charge cycles. Although the direct and precise quantitative comparison of the EIS data could be complicated, the measures to keep the geometry and weight of the electrodes very close to each other could allow for the quantitative analysis of the EIS data.[34,35] Fig. 9 presents the typical Nyquist plots for these systems illustrating their impedance trends upon cycling. The Nyquist plots of both cathodes consist of compressed semicircles in the high (HF) to medium (MF) frequency range, which could be related to the interfacial charge transfer impedance.[34–36] It can be seen (Fig. 9a and the inset) that the EIS spectra of the ternary composite cathode consist of two compressed semicircles at the high to medium frequency part of EIS, and their total impedance was much smaller (three times for the fresh cells and more than ten times for the cycled cells) than the impedance of a single semicircle of the binary composite (Fig. 9b), *i.e.* the addition of $Mg_{0.6}Ni_{0.4}O$ to the S composite cathode significantly reduces its charge transfer resistance. This observation agrees well with the CV data above showing the electrochemical response improvement in the case of the ternary composite. The appearance of an additional semicircle in the ternary composite Nyquist plot could be due to the effect of charge transfer through new boundaries formed by the addition of $Mg_{0.6}Ni_{0.4}O$.

In the EIS spectra of the S/PAN/$Mg_{0.6}Ni_{0.4}O$ composite cathode, the semicircle part is followed by a declined line of the Warburg impedance attributed to the bulk diffusion resistance of the composite cathode.[34–38] The Nyquist plot of the binary S/PAN composite (Fig. 9b) has been developed differently, and the lower frequency part of the spectra is represented by a complex curve, which could be due to the high bulk impedance of S/PAN. The EIS development upon cycling for the binary and ternary composite cathodes could be compared from the data shown in Fig. 9. The binary composite (Fig. 9b) exhibits a high charge transfer resistivity, which remarkably increases upon initial cycling and further slightly reduces and stabilizes at the values much higher than that for the fresh cell. This behavior could be explained by the active material agglomeration observed by SEM (Fig. 6), when the system resistivity drastically increases due to the separation of low conductive S and PAN from other cathode components, and especially from the conductive carbon. In contrast, the charge transfer impedance of the ternary composite (Fig. 9a) rapidly reduces within a few initial cycles and stabilizes at the values much lower than that of the fresh battery. The EIS data show that the $Mg_{0.6}Ni_{0.4}O$ additive significantly improves the charge transfer properties of the composite cathode, which leads to its enhanced electrochemical performance.

The experimental EIS data for the S/PAN/$Mg_{0.6}Ni_{0.4}O$ composite were used for the equivalent circuit analysis. The studied system consisted of multiple interfacial borders and its quantitative analysis could be complicated. However, the EIS spectra analysis could provide valuable information on the additives and surface treatment effects on the interfacial stability of an electrochemical system, their charge transfer properties and electrochemical performance.[34–38] As it can be seen from Fig. 9a and its inset the EIS spectra of a fresh cell with the S/PAN/$Mg_{0.6}Ni_{0.4}O$ cathode are represented by two semicircles in the high and medium frequency range, respectively, followed by a declined line of the Warburg impedance in the low frequency part of EIS. The total impedance in the high to medium frequency range of EIS reduces upon a few initial cycles, which could be attributed to the development of a conductive solid electrolyte interface (SEI). One can see from the inset of Fig. 9a that the high frequency semicircle becomes more distinguished and separated from the medium frequency semicircle, and both the sizes of HF and MF semicircles stabilize within a few initial cycles. Fig. 10 shows the best fitting equivalent circuit along with the fitting results.

The fitting equivalent circuit could be considered as a derivative of the Randles circuit with an additional 'interface element' Q/R and it is represented as follows:

$$R_1 + Q_1/R_2 + Q_2/R_3 + W \quad (1)$$

where R_1, R_2, R_3 are the ohmic resistances at the interfaces, Q_1 and Q_2 are the constant phase elements (CPE) responsible for

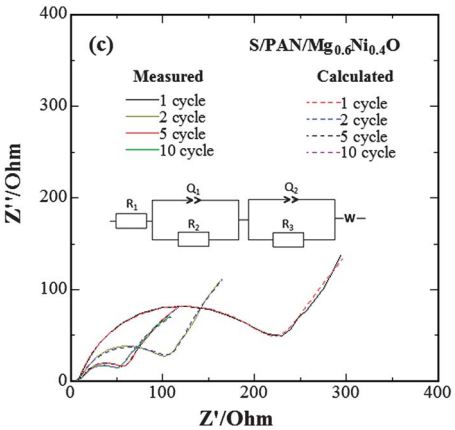

Fig. 10 Equivalent circuit used for fitting the EIS data for the ternary composite.

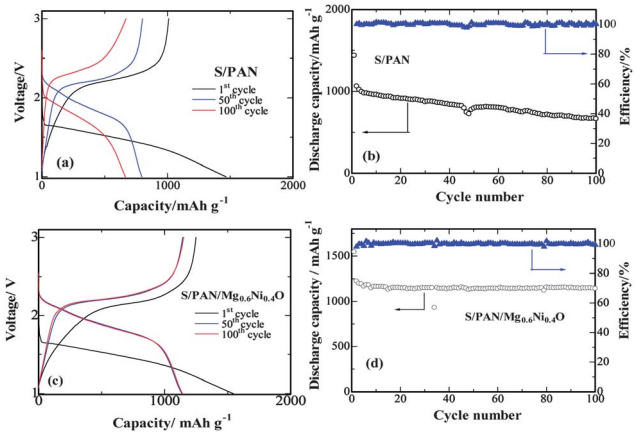

Fig. 11 Discharge–charge profiles, cyclability and capacity retention of the cells with (a and b) binary and (c and d) ternary composite cathodes at 0.1 C.

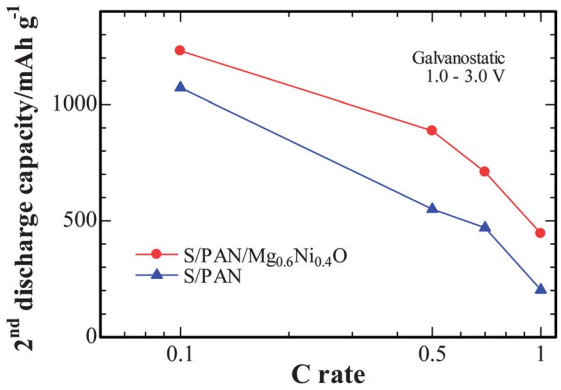

Fig. 12 Rate capability of lithium cells with the S/PAN binary and the S/PAN/$Mg_{0.6}Ni_{0.4}O$ ternary composite cathodes at 0.1 C, 0.5 C, 0.7 C and 1 C.

the double layer capacitance components of the system impedance, and W is the Warburg impedance. It can be seen that the chosen multi-component equivalent circuit fits well with the experimental data (fitting goodness close to 1) and could be used for the qualitative characterization of the studied system. The changes in the circuit component parameters are monitored upon cycling. It is found that while component R_1 has not been remarkably charged upon the battery operation, resistance R_2 is gradually increased (within 10% of its initial value) and the impedance represented by R_3 is remarkably reduced during a few initial cycles. Upon further cycling, the R_1 and R_3 components are stabilized and do notchange noticeably. The constant phase element values slightly change during the first cycle, and are not influenced by the following cycle. The changes in the Warburg impedance were not remarkable. The comparative analysis of the experimental EIS data and the equivalent circuit fitting results allow us to assign the element Q_1/R_2 to the small high frequency (HF) semicircle responsible for the electrode–electrolyte interface impedance,[35,39] and the Q_2/R_2 element of the equivalent circuit is assigned to the following medium frequency (MF) semicircle responsible for the charge transfer resistance.[39] It could be suggested that the interfaces in the system are stabilized upon a few initial discharge–charge cycles, and stable and conductive layers are formed at the electrode–electrolyte interface, favoring the electrochemical stability of the system, and easy charge transfer. This could be considered as one of the reasons for the electrochemical performance stabilization and improved cyclability of the cathode.

The effect of the $Mg_{0.6}Ni_{0.4}O$ addition on the electrochemical performance of the composite cathode can be seen from the discharge–charge profiles, the cyclability and capacity retention data presented in Fig. 11.

It can be seen that the discharge–charge polarization of the ternary composite (Fig. 11c) has been reduced compared with that of the binary cathode (Fig. 11a), which is indicated by a decrease of the voltage gap between the charge and discharge processes, which was observed in the CV data presented in Fig. 8 as well. The kinetics improvement and the polarization decrease achieved in the system by the addition of $Mg_{0.6}Ni_{0.4}O$ could be very beneficial for the utilization of the low-conductive sulfur active material in the composite cathode, and consequently improve the energy and power density of the battery. The ternary S/PAN/$Mg_{0.6}Ni_{0.4}O$ cathode exhibits enhanced electrochemical performance. A specific capacity of 1545 mA h g^{-1} is delivered in the first discharge, and a reversible capacity of 1223 mA h g^{-1} is obtained for a lithium cell with this cathode in the second cycle, and the cell retained about 100% of its initial reversible discharge capacity after 100 cycles. Although both cathodes exhibit high coulombic efficiency (about 100%) over 100 cycles, which could be attributed to the shuttle effect suppression in the S/PAN composite,[23] the binary composite suffers from a very quick capacity fading and the cell with the S/PAN electrode loses about 40% of its initial capacity after 100 cycles of discharge–charge.

The kinetic behaviour of the S/PAN/$Mg_{0.6}Ni_{0.4}O$ composite is further evaluated. The rate capability of the cells with the S/PAN composite and the S/PAN/$Mg_{0.6}Ni_{0.4}O$ composite was examined, respectively. The results for different C rates, namely 0.1, 0.5, 0.7 and 1 C are shown in Fig. 12. For both types of the cells, the capacity decreases gradually with the increase in the discharge–charge current. It is obvious that the cell with the S/PAN/$Mg_{0.6}Ni_{0.4}O$ composite cathode shows an enhanced rate capability. This is, again, due to the significant improvement of the charge transfer properties of the composite cathode and its stability by the $Mg_{0.6}Ni_{0.4}O$ additive observed in this work.

Conclusions

$Mg_{0.6}Ni_{0.4}O$ powders were successfully synthesized *via* the SHS method followed by a heat treatment. The prepared $Mg_{0.6}Ni_{0.4}O$ powder was used as the additive to the S/PAN composite cathode, and exhibited its high effectiveness to improve the composite morphology stability, chemical uniformity and electrochemical performance. This additive led to the formation of the nanostructured composite and prevented the sulfur agglomeration upon cycling, allowing enhanced sulfur utilization. The CV data showed a noticeable polarization reduction in S/PAN/$Mg_{0.6}Ni_{0.4}O$ compared with the parent (non-additive) S/

PAN cathode indicating the electrochemical kinetics improvement. The EIS experiments and analysis have confirmed these results and revealed remarkable charge transfer impedance reduction by the $Mg_{0.6}Ni_{0.4}O$ additive. These enhanced physical and electrochemical properties allowed an initial reversible discharge capacity of 1223 mA h g^{-1} to be achieved, and the retention of this capacity over 100 cycles at 0.1 C rate along with the coulombic efficiency of about 100%. Furthermore, the cathode rate capability has been remarkably improved by the addition of $Mg_{0.6}Ni_{0.4}O$. The results of this study allow us to conclude that the $Mg_{0.6}Ni_{0.4}O$ powders synthesized *via* the SHS method are very effective additives in preparation of the high performance cathodes for Li/S batteries.

Acknowledgements

This research was financially supported by Positec, Natural Sciences and Engineering Research Council of Canada (NSERC), Canadian Foundation for Innovation (CFI) and the Canada Research Chairs (CRC). The EM research described in this paper was performed at the Canadian Centre for Electron Microscopy at McMaster University, which is supported by NSERC and other government agencies. One of the authors (YZ) thanks the China Scholarship Council for the Study Abroad Scholarship. ZB acknowledges the Seed Grant support from Nazarbayev University.

Notes and references

1 M. Armand and J. M. Tarascon, *Nature*, 2008, **451**, 652.
2 R. P. Tischer, *The Sulfur Electrode*, Academic Press, New York, 1983.
3 P. G. Bruce, S. A. Freunberger, L. J. Hardwick and J. M. Tarascon, *Nat. Mater.*, 2012, **11**, 19.
4 D. Marmorstein, T. H. Yu, K. A. Striebel, F. R. McLarnon, J. Hou and E. J. Cairns, *J. Power Sources*, 2000, **89**, 219.
5 H. Yamin and E. Peled, *J. Power Sources*, 1983, **9**, 281.
6 R. D. Rauh, K. M. Abraham, G. F. Pearson, J. K. Surprenant and S. B. Brummer, *J. Electrochem. Soc.*, 1979, **126**, 523.
7 H. Yamin, A. Gorenshtein, J. Penciner, Y. Sternberg and E. Peled, *J. Electrochem. Soc.*, 1988, **135**, 1045.
8 J. Shim, K. A. Striebel and E. J. Cairns, *J. Electrochem. Soc.*, 2002, **149**, A1321.
9 S. E. Cheon, K. S. Ko, J. H. Cho, S. W. Kim, E. Y. Chin and H. T. Kim, *J. Electrochem. Soc.*, 2003, **150**, A796.
10 J. L. Wang, J. Yang, J. Y. Xie, N. X. Xu and Y. Li, *Electrochem. Commun.*, 2002, **4**, 499.
11 S. C. Han, M. S. Song, H. Lee, H. S. Kim, H. J. Ahn and J. Y. Lee, *J. Electrochem. Soc.*, 2003, **150**, A889.
12 W. Zheng, Y. W. Liu, X. G. Hu and C. F. Zhang, *Electrochim. Acta*, 2006, **51**, 1330.
13 L. X. Yuan, H. P. Yuan, X. P. Qiu, L. Q. Chen and W. T. Zhu, *J. Power Sources*, 2009, **189**, 1141.
14 S. R. Chen, Y. P. Zhai, G. L. Xu, Y. X. Jiang, D. Y. Zhao, J. T. Li, L. Huang and S. G. Sun, *Electrochim. Acta*, 2011, **66**, 9549.
15 J. Wang, S. Y. Chew, Z. W. Zhao, S. Ashraf, D. Wexler, J. Chen, S. H. Ng, S. L. Chou and H. K. Liu, *Carbon*, 2008, **46**, 229.
16 B. Zhang, X. Qin, G. R. Li and X. P. Gao, *Energy Environ. Sci.*, 2010, **3**, 1531.
17 B. Zhang, C. Lai, Z. Zhou and X. P. Gao, *Electrochim. Acta*, 2009, **54**, 3708.
18 H. L. Wang, Y. Yang, Y. Y. Liang, J. T. Robinson, Y. G. Li, A. Jackson, Y. Cui and H. J. Dai, *Nano Lett.*, 2011, **11**, 2644.
19 L. Ji, M. Rao, H. Zheng, L. Zhang, Y. Li, W. Duan, J. Guo, E. J. Cairns and Y. Zhang, *J. Am. Chem. Soc.*, 2011, **133**, 18522.
20 J. Guo, Y. Xu and C. Wang, *Nano Lett.*, 2011, **11**, 4288.
21 L. Ji, M. Rao, S. Aloni, L. Wang, E. J. Cairns and Y. Zhang, *Energy Environ. Sci.*, 2011, **4**, 5053.
22 L. Xiao, Y. Cao, J. Xiao, B. Schwenzer, M. H. Engelhard, L. V. Saraf, Z. Nie, G. J. Exarhos and J. Liu, *Adv. Mater.*, 2012, **24**, 1176.
23 J. L. Wang, J. Yang, C. R. Wan, K. Du, J. Y. Xie and N. X. Xu, *Adv. Funct. Mater.*, 2003, **13**, 487.
24 J. Wang, J. Chen, K. Konstantinov, L. Zhao, S. H. Ng, G. X. Wang, Z. P. Guo and H. K. Liu, *Electrochim. Acta*, 2006, **51**, 4634.
25 M. M. Sun, S. C. Zhang, T. Jiang, L. Zhang and J. H. Yu, *Electrochem. Commun.*, 2008, **10**, 1819.
26 Y. Zhang, Z. Bakenov, Y. Zhao, A. Konarov, T. N. L. Doan, M. Malik, T. Paron and P. Chen, *J. Power Sources*, 2012, **208**, 1.
27 S. C. Han, M. S. Song, H. Lee, H. S. Kim, H. J. Ahn and J. Y. Lee, *J. Electrochem. Soc.*, 2003, **150**, A889.
28 Y. J. Choi, K. W. Kim, H. J. Ahn and J. H. Ahn, *J. Alloys Compd.*, 2008, **449**, 313.
29 M. S. Song, S. C. Han, H. S. Kim, J. H. Kim, K. T. Kim and Y. M. Kang, *J. Electrochem. Soc.*, 2004, **151**, A791.
30 Y. Zhang, X. B. Wu, H. Feng, L. Z. Wang, A. Q. Zhang, T. C. Xia and H. C. Dong, *Int. J. Hydrogen Energy*, 2009, **34**, 1556.
31 B. H. Jeon, J. H. Yeon, K. M. Kim and I. J. Chung, *J. Power Sources*, 2002, **109**, 89.
32 B. H. Jeon, J. H. Yeon and I. J. Chung, *J. Mater. Process. Technol.*, 2003, **143–144**, 93.
33 A. Evans, M. I. Montenegro and D. Pletcher, *Electrochem. Commun.*, 2001, **3**, 514.
34 Z. Bakenov and I. Taniguchi, *J. Electrochem. Soc.*, 2010, **157**, A430.
35 Z. Bakenov and I. Taniguchi, *J. Power Sources*, 2010, **195**, 7445.
36 J. W. Choi, J. K. Kim, G. Cheruvally, J. H. Ahn, H. J. Ahn and K. W. Kim, *Electrochim. Acta*, 2007, **52**, 2075.
37 Y. J. Choi, Y. D. Chung, C. Y. Baek, K. W. Kim, H. J. Ahn and J. H. Ahn, *J. Power Sources*, 2008, **184**, 548.
38 S. K. Martha, B. Markovsky, J. Grinblat, Y. Gofer, O. Haik, E. Zinigrad, D. Aurbach, T. Drezen, D. Wang, G. Deghenghi and I. Exnar, *J. Electrochem. Soc.*, 2009, **156**, A541.
39 Z. Bakenov, M. Wakihara and I. Taniguchi, *J. Solid State Electrochem.*, 2008, **12**, 57.